Journal of Energy Storage 19 (2018) 28–34

Contents lists available at ScienceDirect

Journal of Energy Storage

journal homepage: www.elsevier.com/locate/est

Integration of supercapacitors into printed circuit boards

Dina Ibrahim Abouelamaiem[a], Lara Rasha[a], Guanjie He[b], Tobias P. Neville[a], Jason Millichamp[a], Tom J. Mason[a], Ana Belen Jorge[c], Ivan P. Parkin[b], Maria-Magdalena Titirici[d], Rongfang Wang[e], Shan Ji[f], Paul R. Shearing[a], Daniel J.L. Brett[a,*]

[a] Electrochemical Innovation Lab, Department of Chemical Engineering, University College London, London, WC1E 7JE, UK
[b] Christopher Ingold Laboratory, Department of Chemistry, University College London, London, WC1H 0AJ, UK
[c] Materials Research Institute, School of Engineering and Materials Science, Queen Mary University of London, London, E1 4NS, UK
[d] Centre of Functional Nanomaterials, School of Engineering and Materials Science, Queen Mary University of London, Queen Mary University of London, London, E1 4NS, UK
[e] Qingdao University of Science and Technology, Institute of Chemical Engineering, Qingdao, China
[f] College of Biological, Chemical Sciences and Engineering, Jiaxing University, 314001, China

ARTICLE INFO

Keywords:
Activated carbon
Hybrid systems
Printed circuit board
Supercapacitor
Integrated energy storage
Wearable power systems

ABSTRACT

Physically integrated energy storage devices are gaining increasing interest due to the rapid development of flexible, wearable and portable electronics technology. For the first time, supercapacitor components have been integrated into a printed circuit board (PCB) construct. This proof-of-concept study paves the way for integrating supercapacitors into power electronics devices and hybridising with PCB fuel cells. Commercial Norit activated carbon (NAC) was used as the electrode material and was tested in two types of electrolytes, sodium sulfate (Na_2SO_4) aqueous electrolyte, and Na_2SO_4-polyvinyl alcohol (Na_2SO_4-PVA) gel electrolyte. Electrochemical measurements compare the SC-PCBs to standard two-electrode button-cell supercapacitors. A volumetric energy density of 0.56 mW h cm^{-3} at a power density of 26 mW cm^{-3} was obtained in the solid-state SC-PCB system, which is over twice the values acquired in the standard cell configuration. This is due to the removal of bulky components in the standard cell, and/or decreased thickness of the overall device, and thus a decrease in the total volume of the SC-PCB configuration. The results show great potential for embedding supercapacitors into PCBs for a broad range of applications. In addition, further advantages can be realised through close physical integration with other PCB-based electrochemical power systems such as fuel cells.

1. Introduction

Supercapacitors (SC), also known as electrochemical capacitors or ultracapacitors, are charge-storage devices, consisting of two parallel electrodes, an electrolyte and usually a separator that electrically isolates the electrode compartments [1]. Supercapacitors have gained increasing interest in a range of applications including automotive and hybrid electrochemical systems due to their long cycle life, rapid charging-discharging and high power density compared to batteries [2,3]. However, the major drawback of supercapacitors is their low energy density, and hence the development of new electrode materials to meet the requirements of both high energy and power densities is gaining increasing interest [4]. Supercapacitors are classified into two main categories: i) electrical double-layer capacitors (EDLCs), mainly comprising of carbon materials, in which the charge is stored electrostatically at the electrode surface, and ii) pseudo-capacitors, including metal oxides and conductive polymers, whereby Faradaic reversible reactions between the electrode materials and the electrolyte ions, govern the charging and discharging mechanism [5]. Hybrid SCs with asymmetrical configurations have recently gained increasing interest, offering higher energy and power densities [6–8]. While extensive research has been, and continues to be, dedicated to developing improved materials for supercapacitors, much less attention has gone into looking at how they are packaged and physically integrated with other power sources to form unitised hybrid systems. This proof-of-concept study shows how supercapacitors can be integrated into printed circuit board (PCB) structures. The PCB construct offers a low-cost easily manufactured means of making supercapacitors and can directly integrate supercapacitors with PCB fuel cells to make for a highly flexible hybrid power source.

The advantages associated with integrating fuel cells into PCBs are well known. Polymer electrolyte membrane fuel cells (PEMFC), direct

* Corresponding author.
E-mail address: d.brett@ucl.ac.uk (D.J.L. Brett).

https://doi.org/10.1016/j.est.2018.06.016
Received 30 March 2018; Received in revised form 17 May 2018; Accepted 26 June 2018

formic acid fuel cells (DFAFC) and direct ethanol fuel cells have been fabricated using the printed circuit board (PCB) technology [9–12], and the approach is being commercialized by the likes of Bramble Energy in the UK [13]. Printed circuit boards typically consist of fiberglass/epoxy composites, coated with a thin layer of conductive copper [14]. The flow-field can be constructed from the insulating composite and the conducting layer (typically protected with an anti-corrosive layer) can act as the current collector. The PCB approach to constructing fuel cells provides a range of advantages, including robustness, rapid manufacture times, low cost and design flexibility [10]. The scope of integrating fuel cell and supercapacitor technology into a single integrated construct offers the opportunity to improve fuel cell performance with only marginal increases in cost, weight and volume.

While the concept of PCB encapsulated capacitors has been asserted in the patent literature [15,16], to our knowledge this is the first time that a supercapacitor PCB has been demonstrated.

Supercapacitors using commercially available carbon electrodes have demonstrated good specific capacitances as high as 120 F g^{-1} in aqueous electrolyte [17–19], in addition to high power densities ranging between 10 and 20 kW kg^{-1} [20,21]; such standard materials have therefore been used for integration into PCB composites using neutral electrolyte without a separator. In addition, an all-solid-state supercapacitor PCB has been fabricated using a gel electrolyte. Results are compared using the same materials in standard coin cells.

2. Experimental

2.1. Materials

Norit activated carbon (NAC) was provided by CABOT Corporation (Georgia, USA). Polyvinylidene fluoride (PVDF) was supplied by PI-KEM Ltd. (Staffordshire, UK) and Whatman glass microfiber filter papers, used as electrical separator materials, were purchased from Sigma-Aldrich Ltd (UK). Sodium sulphate (Na_2SO_4) and polyvinyl alcohol (PVA) were used as electrolytes in the PCBs and were supplied by Fisher Scientific (UK) and Tokyo Chemical Industry Co. Ltd (Japan), respectively. All prepared electrodes were manually cast on an Arlon DiClad PCB configuration manufactured by Arlon Electronic Materials (UK) and supplied by ZOT Engineering Limited (UK). The pre-impregnated (prepreg) composite bonding fibers, (Arlon-47 N) were also manufactured by Arlon Electronic Materials (UK) and supplied by ZOT Engineering Limited (UK). Nickel foam (Suzhou JSD Co. Ltd., China) was used as the current collector in coin cell devices of CR2032 geometry (Hohsen Corporation, Japan).

2.2. Preparation of electrode materials and gel electrolyte

Commercial carbon, NAC, was used as the electrode material and was mixed with PVDF binder with 95:5 wt.% composition in N-methyl-2-pyrrolidine (NMP) solvent. The carbon pastes were manually cast onto the PCB, and on nickel foam current collector for the coin cell devices, to obtain a constant mass loading of 2 mg cm^2 of active electrode materials.

The flexible gel electrolyte was prepared by mixing 6 g PVA powder in 60 ml deionised water using magnetic stirring at 90 °C. 6 g of 0.5 M Na_2SO_4 was subsequently added to the mixture and stirred until the solution became clear.

2.3. PCB properties and assembly of the supercapacitor-PCBs

The 0.42 mm thick DiClad PCBs (85 mm × 70 mm circuit size) were used as supplied. The DiClad laminates, composed of woven fiberglass/polytetrafluoroethylene (PTFE) composites were used as the substrate for the PCB devices. A thin copper film (38 μm) was electrodeposited on one side of each of the laminates, to provide electrical conductivity, and a conductive carbon ink, which acts as a current collector for the supercapacitor PCBs (SC-PCBs), was coated on top of the copper with a thickness of 35.5 μm and 4 cm diameter circle. The prepared carbon electrode pastes were cast on the conductive ink area and vacuum dried overnight to give a final total mass of 2 mg cm^{-2} of physical surface area. Fig. 1 and S1 illustrate the PCB design used prior to assembly.

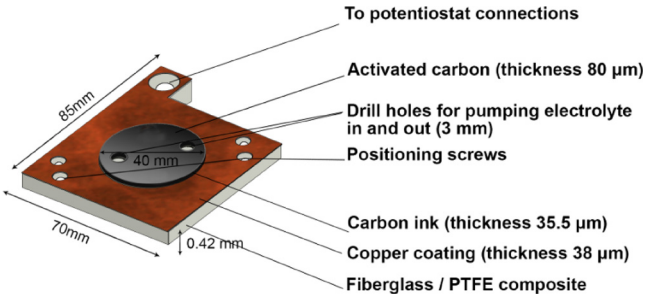

Fig. 1. PCB layout constituting the base of fiberglass/PTFE composite, a thin layer of copper coating along with another layer of carbon ink on which the activated carbon is deposited on.

For the PCB device in aqueous electrolyte medium, the electrode-coated DiClads were separated by two A-47 N prepregs, each of 80 μm thickness, prior to hot pressing. The prepregs were laser-cut to the same dimensions of the PCBs using a CO_2 laser cutter/engraver LS3020 (HPC Laser Ltd, UK) and pre-vacuumed at room temperature for 2 h. The whole device, composed of the PCB and two prepregs, was then hot pressed at 140 °C (curing temperature of prepregs) at a pressure of 2 bar for 1 h in a multilayer press (RMP 210, Bungard, Germany). The final thickness of each of the prepregs ranged between 40 μm and 50 μm after the curing process in the hot press. The SC-PCB device was then irrigated with 0.5 M Na_2SO_4 solution via an access hole in the PCB which was subsequently taped to prevent any electrolyte loss.

The all-solid-state PCB was prepared using the same procedure as the aqueous one without using the prepregs material. The Na_2SO_4-PVA gel electrolyte was placed between both electrodes along with Whatman filter papers, acting as a separator and gently pressed. Fig. 2a and b demonstrates the layering of the two different configurations of the supercapacitor PCB assemblies, with gel and aqueous electrolytes, respectively.

2.4. Characterization

Suitable characterization of the electrode materials used in the SC-PCB was necessary in order to make a fair comparison with other systems reported in the literature. The surface morphology of the activated carbon was examined using scanning electron microscopy (SEM) operating at 10 kV (EVO MA10, ZEISS, Germany). Degassing of the carbon sample at 300 °C using a sample degas system (VacPrep 061 Sample Degas System, Micrometrics, USA) was followed by collection of nitrogen sorption isotherms (3Flex Surface and Catalyst Characterization System, Micromeritics, USA). The total pore volume of the activated carbon was calculated at a relative pressure (P/P_o) of 0.99 and specific surface areas (SSA) were obtained using Brunauer-Emmet-Teller (BET) method at relative pressure range between 0.001 and 0.2 [22]. Non-local density functional theory (NLDFT) was used to determine the micropore volume [23].

2.5. Electrochemical measurements

Electrochemical measurements were carried out in the aqueous and all-solid-state coin cell configurations and SC-PCBs using a potentiostat (Interface 1000, Gamry Instruments, USA). Cyclic voltammetry (CV) at scan rates of 1, 2, 5, 10, 50, 100 and 200 mV s^{-1} were performed in the voltage range 0−2 V.

The specific capacitance was evaluated from the CV curves using Eq. (1):

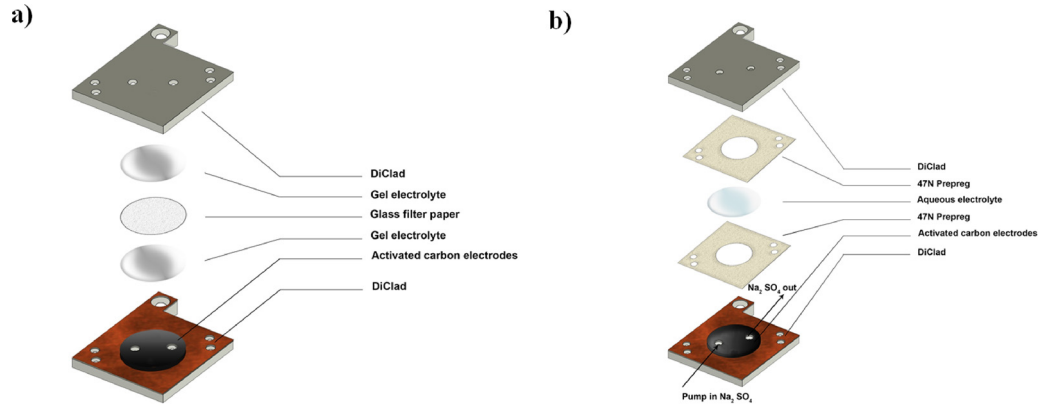

Fig. 2. Schematic of the SC-PCBs: a) as an all-solid-state PCB using a gel electrolyte and b) in aqueous media.

$$C_s = \frac{1}{2}\frac{\int I(V)dV}{s\,\Delta V\,m} \quad (1)$$

where I is the current (A), V is the voltage (V), s is the sweep rate of the cyclic voltammogram (V s^{-1}), ΔV is the voltage range the sweep is carried within (V), and m is the mass of the electrode materials (g).

Galvanostatic charge-discharge cycles (GCD) at current densities ranging between 1 A g^{-1} and 20 A g^{-1} (when possible) were conducted, and the specific capacitances (C_s) were calculated from the GCD curves for comparison to the values attained by CV measurements using Eq. (2):

$$C_s = \frac{i\,\Delta t}{\Delta V} \quad (2)$$

where i is the current density (A g^{-1}), Δt is the time (s) needed for the discharge half-cycle, and ΔV is the voltage range (V) in which the cycling is applied.

The energy density (E) and power density (P) based on the area specific volume of the device (SC-PCB or coin cell) on which the carbon electrodes have been coated (without including the edge material) were obtained from Eqs. (3) and (4):

$$E = \frac{1}{2}C\frac{V^2}{3600\,v} \quad (3)$$

$$P = \frac{E}{\Delta t} \quad (4)$$

where C is the capacitance (F) and v is the volume of the device (cm^3).

The energy density (E_m) and power density (P_m) based on the total mass of the active materials used in the device were calculated following Eqn. (5) and (6):

$$E_m = \frac{1}{2}C_s\,V^2 \quad (5)$$

$$P_m = \frac{E_m}{\Delta t} \quad (6)$$

Potentiostatic electrochemical impedance spectroscopy (EIS) was performed in a frequency range between 0.1 Hz and 1 MHz *vs.* open circuit voltage with an AC perturbation of 10 mV; the different resistances were inferred from the impedance curves.

3. Results and discussion

3.1. Surface morphology characterization

The pore morphology and pore size distribution (PSD) of the commercial carbon NAC was characterized using SEM and nitrogen sorption isotherms, respectively. Table 1 and Fig. S2 and S3 summarize the properties of the activated carbon. It is clear that NAC has a disordered morphology with relatively high SSA and bulk density. However, the values of this activated carbon are lower compared to functionalized carbons with KOH, H_3PO_4 and other activating chemical agents, that reach 3200 $m^2\,g^{-1}$ SSA and 0.91 g cm^{-3} bulk densities [24–28]. The sorption isotherm and NAC exhibit a Type I isotherm, characteristic of microporous solids.

Table 1
Structural properties, including bulk density, SSA determined by BET and total pore volume determined by NLDFT method commercial carbon NAC.

Sample	Bulk Density (g cm^{-3})	SSA ($m^2\,g^{-1}$)	Total Pore Volume ($cm^3\,g^{-1}$)
NAC	0.19	1466	0.74

The major parameters that enhance the electrochemical behaviour of electrode materials in supercapacitor applications include high surface areas, a wide pore size distribution and an interconnected porous structure. In addition, low values of packing density can affect the volumetric energy and power densities of the supercapacitor devices [29]. The effect of these parameters on the electrochemical performance in the coin cells and SC-PCBs is highlighted in the following section.

3.2. Electrochemical characterization

Electrochemical measurements were first conducted in coin cell devices using aqueous and gel electrolytes to assess the performance of the activated carbons in standard operating cells. The coin cells were fabricated in aqueous 0.5 M Na_2SO_4 electrolyte solution and as a solid-state coin cell with Na_2SO_4-PVA gel electrolyte. The total mass loading of the active material was similar to that used in the SC-PCBs. The electrochemical performance of both NAC coin cells is presented in Figs. 3, 4, and S4. NAC exhibited a stable performance in the voltage range of 0−2 V in the aqueous electrolyte with a CV profile approaching a rectangular shape, in comparison with the activated carbon in the gel electrolyte, which presented a quasi-rectangular profile (Fig. 3). The performance of both of the symmetric devices exhibit a profile characteristic of electrical double-layer capacitors [30]. It is note-worthy mentioning that the nickel foam current collector in these configurations has insignificant contribution to the electrochemical behaviour of the activated carbons used (Fig. S5).

The specific capacitance at different sweep rates was evaluated and is reported in Fig. 4a. Both NAC coin cells achieve specific capacitance values of 91 F g^{-1} and 81 F g^{-1} in aqueous and solid systems, respectively, at a scan rate 1 mV s^{-1}. However, the capacitance values maintained 38% in the aqueous Na_2SO_4 electrolyte and 17% in Na_2SO_4-PVA electrolyte, of the initial capacitances upon increasing the sweep rate to 200 mV s^{-1}. The performances in both cells are attributed to the disordered morphology of the activated carbon that does not facilitate the electrolyte diffusion into the micropores and hence the decreased

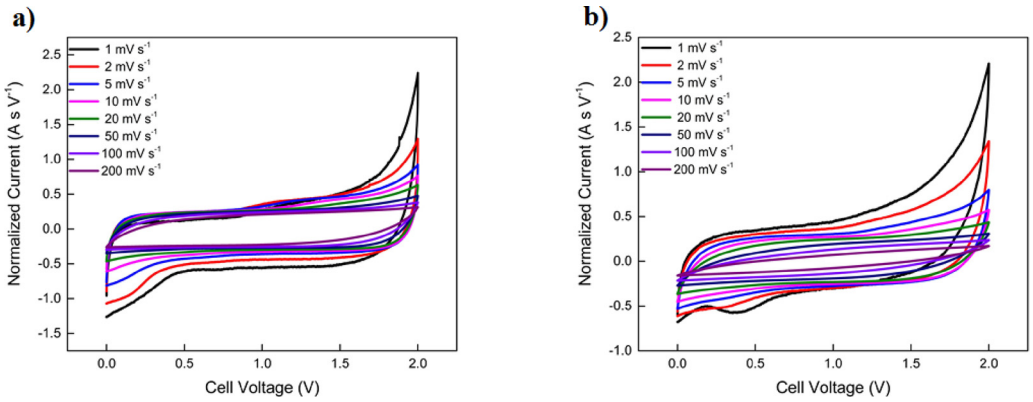

Fig. 3. Normalized cyclic voltammograms of NAC coin cells in a) Na_2SO_4 electrolyte and b) Na_2SO_4-PVA electrolyte at different sweep rates increasing from 1 mV s^{-1} to 200 mV s^{-1}.

performance at high sweep rates [31]. In addition, the poorer performance of the supercapacitor cell in the gel electrolyte is due to the lower ionic conductivity of the gel and the lower wettability at the electrode/electrolyte interface. These results corroborate the GCD experiments conducted at different current densities, shown in Fig. S4. The coin cell configurations recorded almost symmetrical charge-discharge curves with an ohmic drop of 63 mV and 312 mV at 2 A g^{-1} current density in the aqueous and gel electrolytes, respectively. The EIS data confirmed that the impedance values at high frequency are higher for the all-solid-state cell (8.9 Ω cm^2), compared to the coin cell in 0.5 M Na_2SO_4 (1.3 Ω cm^2), shown in Fig. 4b. This revealed that the solid-state coin cell has a higher ohmic resistance due to the relatively low conductivity of the gel electrolyte and poor wettability of the electrode [32].

Upon cycling the coin cells for 5000 charge-discharge cycles, the capacitance retention was found to be 44% for the coin cell in an aqueous medium, and 70% for the solid-state coin cell at 2 A g^{-1} current density (Fig. 5). The limited electrochemical stability is attributed to the disordered structure of the commercial carbons that does not consist of hierarchical porous structures, compared to fabricated carbon materials reported in the literature [33–35]. In addition, the extended potential window up to 2 V might lead to the evolution of nascent gases that abrupt the electrolyte ion diffusion, and therefore diminishes the capacitive performance; although different studies have demonstrated good stability in aqueous Na2SO4 up to 2 V [36–40]. A current leap usually occurs when the cell voltage is extended to 2 V in these electrolytes, demonstrating the gas evolution at the anode and/or cathode, thus implicating lower potential limits to ensure excellent stability and

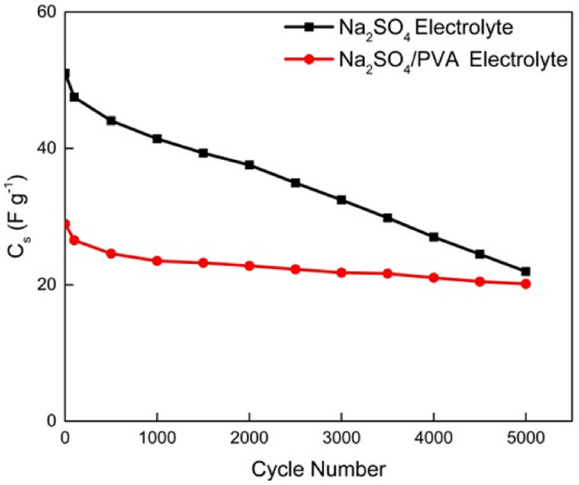

Fig. 5. Cycling stability test of NAC coin cells in Na_2SO_4 and Na_2SO_4-PVA electrolytes.

cyclability of the supercapacitor device [41]. This may be extensively enhanced if carbons with an optimised hierarchical porous network were used as the electrode materials and decreasing the potential window to 1.8 V in the electrolyte media used herein [42–44].

These results set the baseline for coin cell supercapacitor performance using an established carbon electrode material operating in aqueous and solid-state electrolyte systems. The electrochemical

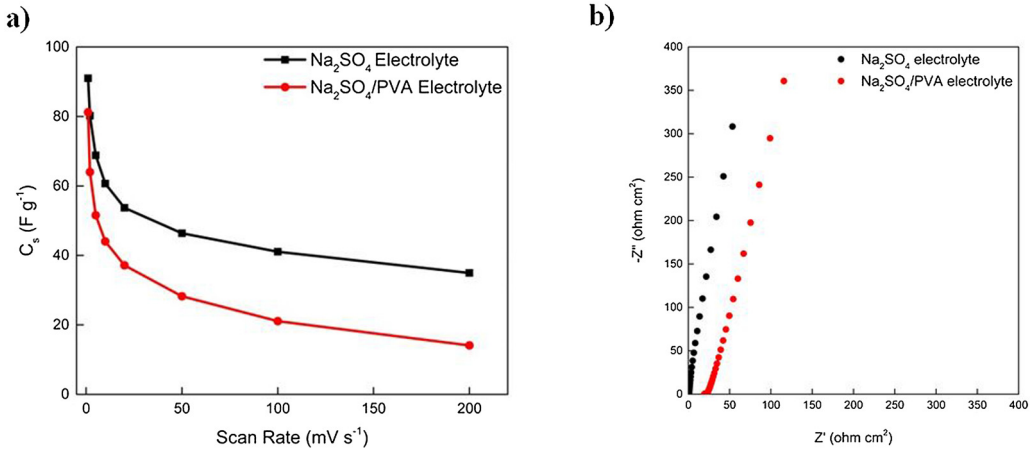

Fig. 4. a) Variation of specific capacitance of NAC coin cells in aqueous Na_2SO_4 and Na_2SO_4-PVA electrolyte with the sweep rate and b) normalized Nyquist plots with the coated surface area of the electrodes of the NAC coin cells comparing two different electrolytes in the frequency range 0.01 Hz–1 MHz.

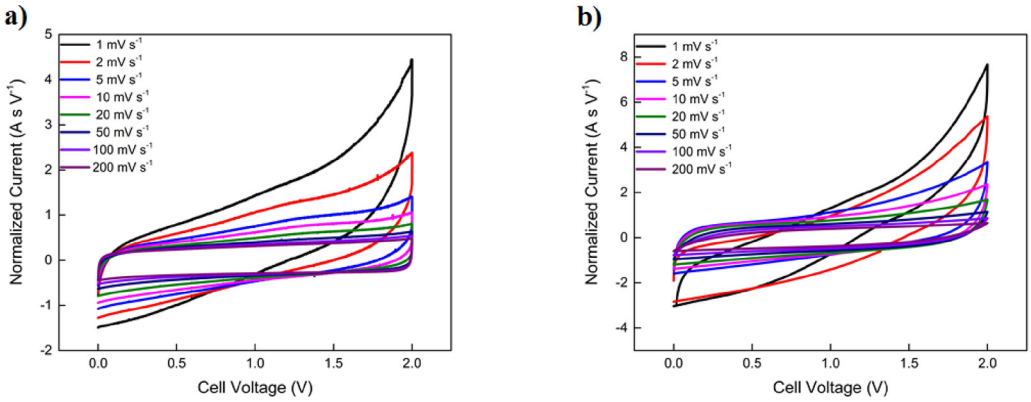

Fig. 6. Normalized cyclic voltammograms of NAC SC-PCBs at different sweep rates increasing from 1 mV s^{-1} to 200 mV s^{-1}, in the voltage range of 0–2 V in a) Na_2SO_4 electrolyte solution and b) Na_2SO_4-PVA electrolyte.

behaviour of SC-PCBs was tested in both aqueous 0.5 M Na_2SO_4 and Na_2SO_4-PVA gel electrolytes. Cyclic voltammograms of the NAC in both electrolyte solutions were performed at a range of scan rates from 1 mV s^{-1} to 200 mV s^{-1} (Fig. 6a, b). NAC exhibited a stable performance in the voltage range of 0–2 V in the aqueous electrolyte with a CV profile of almost rectangular shape, in comparison with the activated carbon in gel electrolyte, which presented a quasi-rectangular profile. The performances of both flexible symmetric devices are characteristic of electrical double-layer capacitors, which is similar to the behaviour obtained in the coin cells. The specific capacitance at a scan rate of 1 mV s^{-1} recorded values of 93 F g^{-1} and 84 F g^{-1} in aqueous and all-solid-state devices, respectively. The results obtained demonstrate that the SC-PCBs can deliver the capacitance achieved in coin cell systems with the same active material and can be optimized with a smaller coating surface area for the carbon electrodes.

Fig. 7a shows that the capacitive performance quickly diminished upon increasing the sweep rate to 5 mV s^{-1} in both electrolytes; however, the values of the specific capacitance decreased gradually with a further increase of the scan rate to 200 mV s^{-1}. This is due to the morphological structure of the activated carbon used as electrode material, previously shown in the coin cell performance.

The GCD curves at different current densities demonstrated almost symmetrical and triangular charge/discharge curves (Fig. S6). A smaller voltage drop (iR drop) of 7 mV at the start point of the discharge curve was obtained in the aqueous system at 2 A g^{-1} current density, compared to 186 mV in the gel electrolyte. EIS plots of the SC-PCB devices, illustrated in Fig. 7b, showed a similar trend for the electrolytes obtained with the GCD curves, with a higher impedance value in the all-solid-state system at high-frequency (10 kHz – 1 MHz). This is usually attributed to the lower conductivity of the gel electrolyte caused by the addition of a polymer and therefore the difference in the bulk electrolyte resistance and electrode/electrolyte resistances between Na_2SO_4 and Na_2SO_4-PVA [45]. The high-frequency impedance (~2.6 Ω cm^2) in the aqueous electrolyte was slightly higher that achieved in the coin cell due to the higher physical surface area of the coated electrodes; however, the high-frequency impedance in the all-solid state device of 21.7 Ω cm^2 was much higher in the SC-PCB device compared to the coin cell with the same electrolyte. These results indicate that the internal resistances at the electrode/electrolyte interface, indicated at high frequency, are higher in the all-solid state SC-PCB, possibly due to the loss of water content upon exposure to air in the SC-PCB and therefore decrease in the ionic mobility and conductivity of the gel electrolyte [46].

Fig. 8 shows that the SC-PCB with the NAC electrodes retained 76% of the initial capacitance in the Na_2SO_4 electrolyte after 5000 charge-discharge cycles at a current density of 2 A g^{-1}. However, SC-PCB in gel electrolyte showed a capacitance retention of 42% of its initial value after the cycling test. The stability of the aqueous system was higher than that acquired in the coin cell, which is likely due to the undesirable evolution of gases in the sealed coin cell system occuring at the upper voltage limit. This causes the rapid degradation of the coin cell performance. On the other hand, the SC-PCB device incorporates drill holes that allow evolved gas to be released from the setup, hence delaying the deterioration of the capacitive performance upon repetitive cycling [47–49]. As for the all-solid state devices, the fully sealed design of the coin cell system ensures that the water content of the gel electrolyte is maintained throughout the cycling test; whereas the ventilated SC-PCB device can lead to electrolyte dehydration and thus diminished wettability and ionic conductivity of the gel upon its complete solidification. The stability of the all-solid-state SC-PCB can be

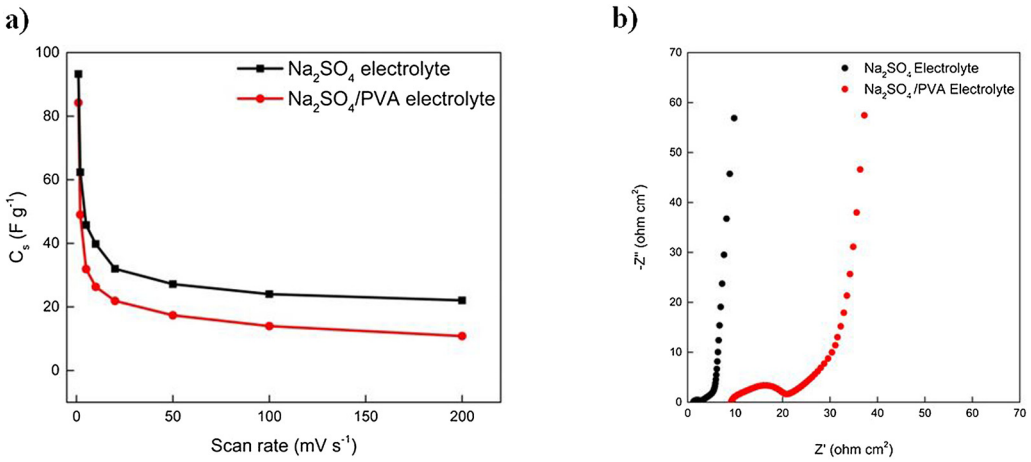

Fig. 7. a) Variation of specific capacitance of NAC SC-PCBs in aqueous Na_2SO_4 and Na_2SO_4-PVA electrolyte with the sweep rate and b) normalized Nyquist plots with the physical coated surface area of the electrodes of NAC SC-PCBs comparing two different electrolytes in the frequency range 0.01 Hz-1 MHz.

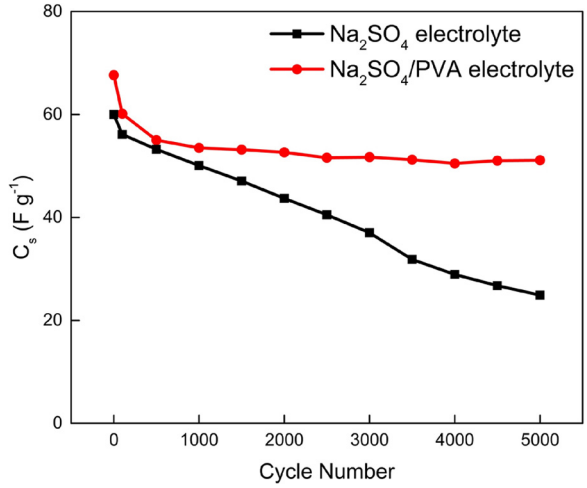

Fig. 8. Cycling stability test up to 5000 cycles of NAC SC-PCBs in Na_2SO_4 and Na_2SO_4-PVA electrolytes.

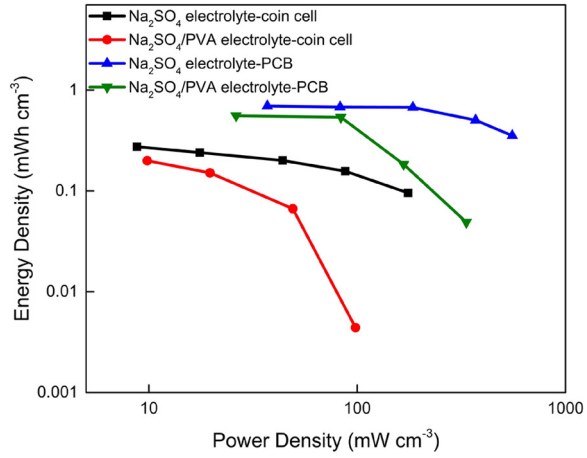

Fig. 9. Ragone plot of the volumetric energy and power densities of the activated carbons in the coin cell and SC-PCB configurations in both electrolytes.

improved by sealing the device and hence maintaining the water content of the gel electrolyte. This boosts the ion mobility, enhancing the conductivity of the gel [46,50].

The volumetric energy densities at different power densities were evaluated for the coin cell and PCB configurations in the different electrolyte media. The Ragone plot of the coin cells in different electrolytes demonstrates that a volumetric energy density of 0.27 mW h cm^{-3} and 0.2 mW h cm^{-3} are achieved at power densities of 8.8 mW cm^{-3} and 9.8 mW cm^{-3}, in the aqueous and solid-state cells, respectively (Fig. 9). The volumetric densities can be further boosted with higher mass loadings of electrode materials whilst maintaining a good capacitive performance [51]. The corresponding gravimetric energy densities achieved were 31.2 Wh $kg^{-1}$and 20.3 Wh kg^{-1} at a power density of 1 kW kg^{-1} in the aqueous and all-state coin cells, respectively (Fig. S7). The values achieved herein are higher than those reported in the literature for the same activated carbon due to the extended potential window of 2 V used in different electrolyte media [18,52].

In both electrolyte media, higher volumetric energy densities are achieved in the SC-PCBs compared to the coin cell devices. The aqueous and all-solid-state SC-PCBs achieved an energy density of 0.69 mW h cm^{-3} and 0.56 mW h cm^{-3} at a power density of 37 mW cm^{-3} and 26 mW cm^{-3}, respectively. The energy density values do not decrease significantly upon increasing the power density, especially for the SC-PCB in aqueous electrolyte, where an energy density of 0.35 mW h cm^{-3} at 555 mW cm^{-3} power density is achieved. These values are lower than those of the micro-supercapacitor devices reported in the literature [53,54]. Hence, increasing the mass loading per geometric surface area and using electrode materials with higher performance rates (including pseudocapacitive materials) would be the next step in fabricating SC-PCBs with higher performance [55–57].

4. Conclusion

Supercapacitor materials have been integrated and tested in a composite printed circuit board construct for the first time. The electrochemical performance of a commercial carbon electrode material with both aqueous and gel electrolyte has been compared with that of a conventional coin cell. The results show that the approach is feasible and can deliver promising performance. Building on this proof-of-concept study, higher performing, state-of-the-art materials, such pseudocapacitive electrode materials, can be used to improve performance and act as a 'drop-in' to the PCB structural hardware. The approach also offers the possibility of integrating both supercapacitor and polymer electrolyte fuel cell into a single flexible design package to bring the best of both power and energy density to a hybridised system.

Acknowledgements

The authors would like to thank the Engineering and Physical Sciences Research (EPSRC) for financial support of electrochemical energy conversion and storage research in the Electrochemical Innovation Lab for support (EP/R023581/1; EP/P009050/1; EP/N032888/1; EP/K014706/2; EP/M014371/1; EP/M023508/1; EP/M009394/1; EP/K038656/1). PRS acknowledges the Royal Academy of Engineering Chair in Emerging Technologies.

Appendix A. Supplementary data

Supplementary material related to this article can be found, in the online version, at doi:https://doi.org/10.1016/j.est.2018.06.016.

References

[1] G. Wang, L. Zhang, J. Zhang, A review of electrode materials for electrochemical supercapacitors, Chem. Soc. Rev. 41 (2) (2012) 797–828.
[2] A. González, E. Goikolea, J.A. Barrena, R. Mysyk, Review on supercapacitors: technologies and materials, Renew. Sustain. Energy Rev. 58 (2016) 1189–1206.
[3] V.V.N. Obreja, On the performance of supercapacitors with electrodes based on carbon nanotubes and carbon activated material—a review, Phys. E 40 (7) (2008) 2596–2605.
[4] Y. Deng, Y. Xie, K. Zou, X. Ji, Review on recent advances in nitrogen-doped carbons: preparations and applications in supercapacitors, J. Mater. Chem. A 4 (4) (2016) 1144–1173.
[5] P.J. Hall, M. Mirzaeian, S.I. Fletcher, F.B. Sillars, A.J.R. Rennie, G.O. Shitta-Bey, et al., Energy storage in electrochemical capacitors: designing functional materials to improve performance, Energy Environ. Sci. 3 (9) (2010) 1238–1251.
[6] D. Yu, K. Goh, Q. Zhang, L. Wei, H. Wang, W. Jiang, et al., Controlled functionalization of carbonaceous fibers for asymmetric solid-state micro-supercapacitors with high volumetric energy density, Adv. Mater. 26 (39) (2014) 6790–6797.
[7] M. Cakici, R.R. Kakarla, F. Alonso-Marroquin, Advanced electrochemical energy storage supercapacitors based on the flexible carbon fiber fabric-coated with uniform coral-like MnO2 structured electrodes, Chem. Eng. J. 309 (2017) 151–158.
[8] W. Ma, S. Chen, S. Yang, W. Chen, W. Weng, Y. Cheng, et al., Flexible all-solid-state asymmetric supercapacitor based on transition metal oxide nanorods/reduced graphene oxide hybrid fibers with high energy density, Carbon 113 (2017) 151–158.
[9] S.H. Kim, H.Y. Cha, C.M. Miesse, J.H. Jang, Y.S. Oh, S.W. Cha, Air-breathing miniature planar stack using the flexible printed circuit board as a current collector, Int. J. Hydrogen Energy 34 (1) (2009) 459–466.
[10] R. O'Hayre, D. Braithwaite, W. Hermann, S.-J. Lee, T. Fabian, S.-W. Cha, et al., Development of portable fuel cell arrays with printed-circuit technology, J. Power Sources 124 (2) (2003) 459–472.
[11] R.I. Jafri, S. Ramaprabhu, Multi walled carbon nanotubes based micro direct ethanol fuel cell using printed circuit board technology, Int. J. Hydrogen Energy 35 (3) (2010) 1339–1346.
[12] P. Hong, S. Liao, J. Zeng, X. Huang, Design, fabrication and performance evaluation of a miniature air breathing direct formic acid fuel cell based on printed circuit board technology, J. Power Sources 195 (21) (2010) 7332–7337.
[13] https://www.brambleenergy.com/.

[14] A. Schmitz, M. Tranitz, S. Wagner, R. Hahn, C. Hebling, Planar self-breathing fuel cells, J. Power Sources 118 (1) (2003) 162–171.
[15] M. Rouvala, T. VON RAUNER, Integration of supercapacitors within a flexible printed circuit and associated methods, Google Patents (2013) US8358110B2.
[16] U. Nortoft, M.T. Jorgensen, O.S. Nissen, Arrangement of electrochemical cells and circuit board, Google Patents (2004) US6773848B1.
[17] E. Raymundo-Piñero, M. Cadek, F. Béguin, Tuning carbon materials for supercapacitors by direct pyrolysis of seaweeds, Adv. Funct. Mater. 19 (7) (2009) 1032–1039.
[18] E.J. Ra, E. Raymundo-Piñero, Y.H. Lee, F. Béguin, High power supercapacitors using polyacrylonitrile-based carbon nanofiber paper, Carbon 47 (13) (2009) 2984–2992.
[19] J. Pokrzywinski, J.K. Keum, R.E. Ruther, E.C. Self, M. Chi, H. Meyer Iii, et al., Unrivaled combination of surface area and pore volume in micelle-templated carbon for supercapacitor energy storage, J. Mater. Chem. A 5 (26) (2017) 13511–13525.
[20] J. Yang, H. Wu, M. Zhu, W. Ren, Y. Lin, H. Chen, et al., Optimized mesopores enabling enhanced rate performance in novel ultrahigh surface area meso-/microporous carbon for supercapacitors, Nano Energy 33 (2017) 453–461.
[21] J. Jian, L. Linpo, L. Yani, L. Siyuan, X. Maowen, Z. Jianhui, Uniform implantation of CNTs on total activated carbon surfaces: a smart engineering protocol for commercial supercapacitor applications, Nanotechnology 28 (14) (2017) 145402.
[22] D.I. Abouelamaiem, G. He, I. Parkin, T.P. Neville, A.B. Jorge, S. Ji, et al., Synergistic relationship between the three-dimensional nanostructure and electrochemical performance in biocarbon supercapacitor electrode materials, Sustain. Energy Fuels 2 (2018) 772–785.
[23] C. Lastoskie, K.E. Gubbins, N. Quirke, Pore size heterogeneity and the carbon slit pore: a density functional theory model, Langmuir 9 (10) (1993) 2693–2702.
[24] H. Wang, Q. Gao, J. Hu, High hydrogen storage capacity of porous carbons prepared by using activated carbon, J. Am. Chem. Soc. 131 (20) (2009) 7016–7022.
[25] A. Alonso, V. Ruiz, C. Blanco, R. Santamaría, M. Granda, R. Menéndez, et al., Activated carbon produced from Sasol-Lurgi gasifier pitch and its application as electrodes in supercapacitors, Carbon 44 (3) (2006) 441–446.
[26] Y. Nakagawa, M. Molina-Sabio, F. Rodríguez-Reinoso, Modification of the porous structure along the preparation of activated carbon monoliths with H3PO4 and ZnCl2, Microporous Mesoporous Mater. 103 (1) (2007) 29–34.
[27] J. Wang, J. Tang, B. Ding, V. Malgras, Z. Chang, X. Hao, et al., Hierarchical porous carbons with layer-by-layer motif architectures from confined soft-template self-assembly in layered materials, Nat. Commun. 8 (2017) 15717.
[28] S. Gao, B.S. Villacorta, L. Ge, K. Steel, T.E. Rufford, Z. Zhu, Effect of rheological properties of mesophase pitch and coal mixtures on pore development in activated carbon discs with high compressive strength, Fuel Process. Technol. 177 (2018) 219–227.
[29] Y. Xu, Z. Lin, X. Zhong, X. Huang, N.O. Weiss, Y. Huang, et al., Holey graphene frameworks for highly efficient capacitive energy storage, Nat. Commun. 5 (2014) 4554.
[30] A. Lewandowski, A. Olejniczak, M. Galinski, I. Stepniak, Performance of carbon–-carbon supercapacitors based on organic, aqueous and ionic liquid electrolytes, J. Power Sources 195 (17) (2010) 5814–5819.
[31] J. Ding, H. Wang, Z. Li, A. Kohandehghan, K. Cui, Z. Xu, et al., Carbon nanosheet frameworks derived from Peat Moss as high performance sodium ion battery anodes, ACS Nano 7 (12) (2013) 11004–11015.
[32] W. Liu, X. Yan, J. Chen, Y. Feng, Q. Xue, Novel and high-performance asymmetric micro-supercapacitors based on graphene quantum dots and polyaniline nanofibers, Nanoscale 5 (13) (2013) 6053–6062.
[33] K. Xia, Q. Gao, J. Jiang, J. Hu, Hierarchical porous carbons with controlled micropores and mesopores for supercapacitor electrode materials, Carbon 46 (13) (2008) 1718–1726.
[34] A.B. Fuertes, G. Lota, T.A. Centeno, E. Frackowiak, Templated mesoporous carbons for supercapacitor application, Electrochim. Acta 50 (14) (2005) 2799–2805.
[35] J. Gamby, P.L. Taberna, P. Simon, J.F. Fauvarque, M. Chesneau, Studies and characterisations of various activated carbons used for carbon/carbon supercapacitors, J. Power Sources 101 (1) (2001) 109–116.
[36] H. Jiang, C. Li, T. Sun, J. Ma, A green and high energy density asymmetric supercapacitor based on ultrathin MnO2 nanostructures and functional mesoporous carbon nanotube electrodes, Nanoscale 4 (3) (2012) 807–812.
[37] Z. Lei, J. Zhang, X.S. Zhao, Ultrathin MnO2 nanofibers grown on graphitic carbon spheres as high-performance asymmetric supercapacitor electrodes, J. Mater. Chem. 22 (1) (2012) 153–160.
[38] K. Fic, G. Lota, M. Meller, E. Frackowiak, Novel insight into neutral medium as electrolyte for high-voltage supercapacitors, Energy Environ. Sci. 5 (2) (2012) 5842–5850.
[39] X. Yang, H. Niu, H. Jiang, Q. Wang, F. Qu, A high energy density all-solid-state asymmetric supercapacitor based on MoS2/graphene nanosheets and MnO2/graphene hybrid electrodes, J. Mater. Chem. A 4 (29) (2016) 11264–11275.
[40] G. Sun, H. Xie, J. Ran, L. Ma, X. Shen, J. Hu, et al., Rational design of uniformly embedded metal oxide nanoparticles into nitrogen-doped carbon aerogel for high-performance asymmetric supercapacitors with a high operating voltage window, J. Mater. Chem. A 4 (42) (2016) 16576–16587.
[41] L. Demarconnay, E. Raymundo-Piñero, F. Béguin, Adjustment of electrodes potential window in an asymmetric carbon/MnO2 supercapacitor, J. Power Sources 196 (1) (2011) 580–586.
[42] H. Wang, Z. Xu, A. Kohandehghan, Z. Li, K. Cui, X. Tan, et al., Interconnected carbon nanosheets derived from hemp for ultrafast supercapacitors with high energy, ACS Nano 7 (6) (2013) 5131–5141.
[43] F. Yu, T. Wang, Z. Wen, H. Wang, High performance all-solid-state symmetric supercapacitor based on porous carbon made from a metal-organic framework compound, J. Power Sources 364 (2017) 9–15.
[44] F. Zhuangjun, Y. Jun, W. Tong, Z. Linjie, N. Guoqing, L. Tianyou, et al., Asymmetric supercapacitors based on Graphene/MnO2 and activated carbon nanofiber electrodes with high power and energy density, Adv. Funct. Mater. 21 (12) (2011) 2366–2375.
[45] M. Kaempgen, C.K. Chan, J. Ma, Y. Cui, G. Gruner, Printable thin film supercapacitors using single-walled carbon nanotubes, Nano Lett. 9 (5) (2009) 1872–1876.
[46] C. Yuan, X. Zhang, Q. Wu, B. Gao, Effect of temperature on the hybrid supercapacitor based on NiO and activated carbon with alkaline polymer gel electrolyte, Solid State Ionics 177 (13) (2006) 1237–1242.
[47] L. Demarconnay, E. Raymundo-Piñero, F. Béguin, A symmetric carbon/carbon supercapacitor operating at 1.6V by using a neutral aqueous solution, Electrochem. Commun. 12 (10) (2010) 1275–1278.
[48] M.P. Bichat, E. Raymundo-Piñero, F. Béguin, High voltage supercapacitor built with seaweed carbons in neutral aqueous electrolyte, Carbon 48 (15) (2010) 4351–4361.
[49] H. Xia, Y.S. Meng, G. Yuan, C. Cui, L. Lu, A symmetric RuO2/RuO2 supercapacitor operating at 1.6 V by using a neutral aqueous electrolyte, Electrochem. Solid State Lett. 15 (4) (2012) A60–A63.
[50] X. Liu, D. Wu, H. Wang, Q. Wang, Self-recovering tough gel electrolyte with adjustable supercapacitor performance, Adv. Mater. 26 (25) (2014) 4370–4375.
[51] J. Zhao, Y. Li, G. Wang, T. Wei, Z. Liu, K. Cheng, et al., Enabling high-volumetric-energy-density supercapacitors: designing open, low-tortuosity heteroatom-doped porous carbon-tube bundle electrodes, J. Mater. Chem. A 5 (44) (2017) 23085–23093.
[52] V. Khomenko, E. Raymundo-Piñero, F. Béguin, High-energy density graphite/AC capacitor in organic electrolyte, J. Power Sources 177 (2) (2008) 643–651.
[53] D. Pech, M. Brunet, H. Durou, P. Huang, V. Mochalin, Y. Gogotsi, et al., Ultrahigh-power micrometre-sized supercapacitors based on onion-like carbon, Nat. Nanotechnol. 5 (2010) 651.
[54] J.Y. Hwang, M. Li, M.F. El-Kady, R.B. Kaner, Next-generation activated carbon supercapacitors: a simple step in electrode processing leads to remarkable gains in energy density, Adv. Funct. Mater. 27 (15) (2017) 1605745.
[55] Z.S. Wu, K. Parvez, X. Feng, K. Müllen, Graphene-based in-plane micro-supercapacitors with high power and energy densities, Nat. Commun. 4 (2013) 2487.
[56] L. Sheng, T. Wei, Y. Liang, L. Jiang, L. Qu, Z. Fan, Vertically oriented graphene nanoribbon fibers for high-volumetric energy density all-solid-state asymmetric supercapacitors, Small 13 (22) (2017) 1700371.
[57] X. Gong, S. Li, P.S. Lee, A fiber asymmetric supercapacitor based on FeOOH/PPy on carbon fibers as an anode electrode with high volumetric energy density for wearable applications, Nanoscale 9 (30) (2017) 10794–10801.